

DeepGDel: Deep Learning-based Gene Deletion Prediction Framework for Growth-Coupled Production in Genome-Scale Metabolic Models

Ziwei Yang¹, Takeyuki Tamura¹

¹ *Bioinformatics Center, Institute for Chemical Research, Kyoto University, Kyoto, Japan*

Abstract—In genome-scale constraint-based metabolic models, gene deletion strategies are crucial for achieving growth-coupled production, where cell growth and target metabolite production are simultaneously achieved. While computational methods for calculating gene deletions have been widely explored and have contributed to gene deletion strategy databases, current approaches remain computationally demanding and have yet to fully leverage emerging data-driven paradigms, such as machine learning, for more efficient strain design. Therefore, it is necessary to propose a fundamental framework for this objective. In this study, we first formulate the problem of gene deletion strategy prediction and then propose a framework for predicting gene deletion strategies for growth-coupled production in genome-scale metabolic models. The proposed framework leverages deep learning algorithms to learn and integrate sequential gene and metabolite data representation, enabling the automatic gene deletion strategy prediction. Computational experiment results demonstrate the feasibility of the proposed framework, showing substantial improvements over baseline methods. Specifically, the proposed framework achieves a 14.69%, 22.52%, and 13.03% increase in overall accuracy across three metabolic models of different scales under study, while maintaining balanced precision and recall in predicting gene deletion statuses. The source code and examples for the framework are publicly available at <https://github.com/MetNetComp/DeepGDel>.

Index Terms—Biology and genetics, Machine learning, Scientific databases, Graphs and networks.

I. INTRODUCTION

Computational approaches play a crucial role in metabolic engineering, enabling the systematic design and optimization of microbial strains [1], [2], [3], [4], [5]. A key application is computational strain design, which leverages mathematical models to simulate metabolism of microorganism and optimize the biosynthesis of target metabolites. Among these models, the **constraint-based model** is widely used in genome-scale metabolic engineering. It consists of two main components: (1) a metabolic network and (2) gene-protein-reaction (GPR) rules. The metabolic network defines the biochemical transformations between metabolites, while enzymatic proteins, encoded by specific genes, catalyze these reactions. GPR rules, expressed as Boolean functions, define the relationships between genes, proteins, and metabolic reactions, specifying whether a reaction remains active based on the presence of specific genes. By modifying the presence of genes, the metabolic network can be systematically reprogrammed. A widely used operation is **gene deletion**, which inactivates specific reactions by removing the genes encoding essential enzymes. This approach is central to metabolic engineering, offering a rational means to rewire metabolism for improved biochemical production.

In the simulation of gene deletions using constraint-based models, the primary objective is to achieve **growth-coupled production** of target metabolites. Growth-coupled production

refers to the coupling of cell growth with the synthesis of target metabolites within microorganisms' metabolic processes. This coupling is critical in industrial applications, as microorganism genotypes with higher growth rates are more likely to outcompete others during repeated passaging, ensuring sustained target metabolite production. However, in the natural metabolic state of most microorganisms, only a limited number of metabolites inherently satisfy the conditions for growth-coupled production. Consequently, it is necessary to design gene deletion strategies to enable growth-coupled production for most target metabolites [6]. To address this challenge, several computational methods have been proposed [7], [8], [9], [10], [11], [12], [13], [14], [15]. In recent years, researchers have successfully applied these gene deletion strategies to real-world challenges, enabling the development of strains for growth-coupled production of target metabolites in biofuel production and the industrial synthesis of platform chemicals [16], [17], [18].

Despite these successes, calculating gene deletion strategies remains computationally demanding, particularly when simulating genome-scale models with complex metabolic networks and GPR rules involving numerous genes. Recent efforts have not only focused on developing new algorithms to optimize these calculations but also on establishing dedicated databases for computational data in strain design. These databases fulfill the growing need for efficient management of gene deletion strategy data and create new opportunities to advance this field. One prominent example is MetNetComp [19], the first web-based platform that curates gene deletion strategies for growth-coupled production in constraint-based metabolic models. MetNetComp computes growth-coupled gene deletion strategies that are either minimal or maximal in terms of the number of gene deletions by modifying the gDel_minRN [15] approach. Currently, it hosts a comprehensive repository of over 85,000 gene deletion strategies for various metabolites across multiple constraint-based models from different species. With the vast gene deletion database now available, there is great potential to explore new paradigms in computational strain design. One of the major challenges presented by this opportunity is how to effectively extract and utilize information from large-scale data to enhance the computational process. A recently proposed gene deletion calculation method, DBgDel [20], attempts to address this to integrate database resources into the calculation. It summarizes known maximal deletion strategies from MetNetComp to refine search spaces during optimization, successfully strike a trade-off between computational time and success rate in genome-scale metabolic models. However, the challenge remains, as this method relies on hand-engineered information extraction rules, which limit the full potential of large-scale datasets. Moreover, it still

depends on downstream gene deletion algorithms to effectively account for GPR rules.

Compared to other related areas in metabolic engineering that have seen some success, effectively integrating available data into computational strain design—particularly through automated, data-driven approaches like machine learning and deep learning [21]—remains largely unexplored. For example, Costello et al. [22] proposed a supervised machine learning model to learn the relationship between metabolites and enzymes from time-series data of protein and metabolite concentrations and to predict target metabolite production; more recently, Li et al. [23] proposed DLKcat, a deep learning-based model that predicts high-throughput enzyme turnover numbers in enzyme-constrained genome-scale metabolic models by learning from substrate structures and protein sequence data. Moreover, recent advances in deep learning have also enabled successful applications in various related domains involving sequential data modeling, beyond metabolic engineering [24], [25].

These success cases demonstrate that advancing this data-driven methodology for gene deletion strategies and computational strain design is also promising. However, this remains a challenging task, as a fundamental framework to achieve this objective is currently absent. To address this gap, a systematic study is needed to cover the process from formulating the task to solving it effectively, with feasibility analysis on the necessary data and suitable computational methods.

In this study, we first formulate the problem of gene deletion strategy prediction and then propose DBgDel, a framework for predicting gene deletion strategies for growth-coupled production in genome-scale metabolic models. DBgDel enables the use of deep learning algorithms to learn from sequential data on genes and metabolites, allowing the automatic prediction of gene deletion strategies for growth-coupled production in a data-driven manner. DBgDel consists of three neural network-based modules: (1) **Meta-M**, which sets up a metabolite representation learning task to learn the characteristics of metabolites in the metabolic model; (2) **Gene-M**, which sets up a gene representation learning task to learn the characteristics of genes in the metabolic model; and (3) **Pred-M**, which integrates the latent representations of metabolite and gene characteristics in a pairwise manner to predict gene deletion states and outputs the final gene deletion strategy.

To the best of our knowledge, this is the first study to formally define the gene deletion strategy prediction task based on prior work in gene deletion calculations and to propose a data-driven prediction framework to address it. Furthermore, the computational experiments demonstrated that the proposed framework effectively predicted gene deletion strategies for growth-coupled production across three metabolic models in a fully data-driven manner, achieving solid performance and outperforming baseline methods in overall accuracy, macro-averaged precision, recall, F1 score, and AUC.

The remaining sections of this paper are organized as follows: Section II-A and II-B formalize the fundamental concepts of this study and illustrate them with a small example; Section II-C defines the primary research problem of this study, namely, the prediction of gene deletion strategies; Section III presents the proposed DBgDel framework along with its implementation details; Section IV-A outlines the setup of the computational experiments; Section IV-B, IV-C, IV-D, and IV-E presents the datasets, baseline methods, and the evaluation metrics used in the experiments; Section IV-F discusses the

TABLE I: Notations used in the definitions in preliminary and problem setting.

Notation	Description
\mathcal{C}	Constraint-based model
\mathcal{C}_1	Metabolic network
\mathcal{C}_2	GPR rule
M	Metabolites in the constraint-based model
R	Reactions in the constraint-based model
V	Reaction rates (flux)
S	Stoichiometry matrix
L	Lower bounds for reaction rates
U	Upper bounds for reaction rates
G	Genes in the constraint-based model
F	Boolean functions for GPR rule
P	Outputs of Boolean functions in F
m_{target}	Target metabolite
r_{target}	Target metabolite production reaction
r_{growth}	Cell growth reaction
$PR_{\text{threshold}}$	Minimum requirement for target production reaction rate
$GR_{\text{threshold}}$	Minimum requirement for cell growth reaction rate
G_{del}	Genes deleted in the gene deletion strategy
DS	Set of gene deletion strategies
DS_{known}	Set of known gene deletion strategies
\widetilde{DS}	Predicted gene deletion strategies
DS^*	Ground-truth strategies corresponding to \widetilde{DS}
$\mathcal{F}(\theta)$	Predictive model parameterized by θ

experimental results, including (1) the performance comparison between the proposed framework and baseline methods, and (2) the performance comparison of DBgDel ablation variants using only sequential gene or metabolite data across the *e_coli_core*, iMM904, and iML1515 metabolic models; Section V analyzes the experimental results, evaluates the performance of DBgDel and its variants, and discusses the limitations and directions for future work.

II. PRELIMINARY AND PROBLEM SETTING

In this section, we first outline several key terms in this study as a preliminary. Next, we define the main problem in this research, namely, **gene deletion strategy prediction**. Finally, we illustrate this concept using a toy constraint-based model. All the notations mentioned in this section are listed in Table I.

A. Preliminary Definition

1) **Constraint-based model**: Let $\mathcal{C} = \{M, R, S, L, U, G, F, P\}$ be a constraint-based model. The elements of \mathcal{C} can be further divided into two parts: (1) the metabolic network and (2) the GPR rule. We describe them as follows:

- **Metabolic network**: Let $\mathcal{C}_1 = \{M, R, S, L, U\}$ be a metabolic network. $M = \{m_1, \dots, m_{|M|}\}$ denotes a set consisting all metabolites, with one of them being the target metabolite m_{target} . $R = \{r_1, \dots, r_{|R|}\}$ denotes a set consisting all reactions, including the cell growth reaction r_{growth} and the target metabolite production reaction r_{target} . To facilitate clarity, we introduce an additional set $V = \{v_1, \dots, v_{|R|}\}$ to represent the reaction rates per unit time (flux) corresponding to reactions in R . Notably, we distinguish the rate of the growth reaction (v_{growth}) as the **Growth Rate (GR)** and that of the target metabolite production reaction (v_{target}) as the **Production Rate (PR)**. The stoichiometry matrix S contains elements $S_{ij} = k$, indicating that reaction r_j either produces (+) or consumes (-) k units of metabolite m_i per unit time. Lower and upper bounds for the

reaction rates for V are denoted by $L = \{l_1, \dots, l_{|R|}\}$ and $U = \{u_1, \dots, u_{|R|}\}$, respectively.

- **GPR rule:** Let $\mathcal{C}_2 = \{G, F, P\}$ be a GPR rule. $G = \{g_1, \dots, g_{|G|}\}$ represents a set of genes, while $F = \{f_1, \dots, f_{|R|}\}$ represents Boolean functions. $P = \{p_1, \dots, p_{|R|}\}$ is a collection of outputs generated by applying the functions in F to the gene set G . Each output p_j can be expressed as $p_j = f_j(G)$, where both p and g are binary values, i.e., $p, g \in \{0, 1\}$. Note that if $p_j = 0$, this imposes a constraint on both the lower bound l_j and the upper bound u_j to be 0, effectively restraining reaction r_j .

2) **Flux balance analysis:** When analyzing the metabolic network within a constraint-based model, flux balance analysis (FBA) assumes steady states where all metabolic reaction speeds (fluxes) are constant [26]. Specifically, we give the following definitions for FBA: (1) for each compound, the sum of the producing fluxes is equal to the sum of the consuming fluxes; (2) in each reaction, the fluxes of substrates and products must satisfy the ratio in the chemical reaction equation, and (3) the upper and lower bounds are given for each flux. In the standard procedure for FBA on the given metabolic network \mathcal{C}_1 , the objective is to maximize the cell growth reaction rate v_{growth} using the following linear programming (LP):

LP Formalization of FBA Using \mathcal{C}_1 of a Constraint-Based Model.

Given: \mathcal{C}_1

Maximize: v_{growth}

1: **Such that:**

2: $\sum_j S_{ij} v_j = 0$ for all i ;

3: $l_j \leq v_j \leq u_j$ for all j ;

4: $i = \{1, \dots, |M|\}, j = \{1, \dots, |R|\}$

3) **Growth-coupled production:** Growth-coupled production is a special situation of microorganism's metabolic processes, wherein the cell growth co-occurs with the synthesis of the target metabolite. In this study, we adopt the paradigm of weakly growth-coupled production, which means achieving a non-zero synthesis rate of the target metabolite at the maximum non-zero growth rate [27], [28]. During the simulation of constraint-based models, growth-coupled production can be defined by two indexes: the lower bound of target metabolite production rate ($PR_{\text{threshold}}$) and the lower bound of cell growth reaction rate ($GR_{\text{threshold}}$). When the GR is maximized, if the simulated values v_{target} and v_{growth} exceed two lower bounds in any cases, respectively, growth-coupled production is considered achieved. In this study, we set $PR_{\text{threshold}} = GR_{\text{threshold}} = 0.001$.

4) **Gene deletion strategy:** In metabolic model simulations and calculations, the gene deletion strategy refers to selecting genes to be deleted to optimize metabolic networks for desired outcomes, such as the growth-coupled production of specific metabolites. The calculation of the gene deletion strategy for growth-coupled production is typically defined as finding a set G_{del} of genes designated for deletion, as presented below:

B. Example

Below is a small example accompanied by explanations to illustrate further the gene deletions in metabolic models.

1) **Toy constraint-based model setup:** Fig. 1 shows a toy example in which $\mathcal{C} = \{M, R, S, L, U, G, F, P\}$ represents a constraint-based model. Specifically, for its

Calculation of Gene Deletion Strategy for Growth-Coupled Production.

Given: \mathcal{C} , r_{target} , $PR_{\text{threshold}}$, $GR_{\text{threshold}}$

Find: $G_{\text{del}} \subset G$ such that $v_{\text{target}} \geq PR_{\text{threshold}}$ and $v_{\text{growth}} \geq GR_{\text{threshold}}$

1: **Such that Minimize:**

2: v_{target}

3: **Such that Maximize:**

4: v_{growth}

5: **Such that:**

6: $\sum_j S_{ij} v_j = 0$ for all i ;

7: $\begin{cases} v_j = 0 & \text{if } p_j = 0, \\ l_j \leq v_j \leq u_j & \text{otherwise;} \end{cases}$

8: $p_j = f_j(G)$;

9: $\begin{cases} g = 0 & \text{if } g \in G_{\text{del}}, \\ g = 1 & \text{otherwise;} \end{cases}$

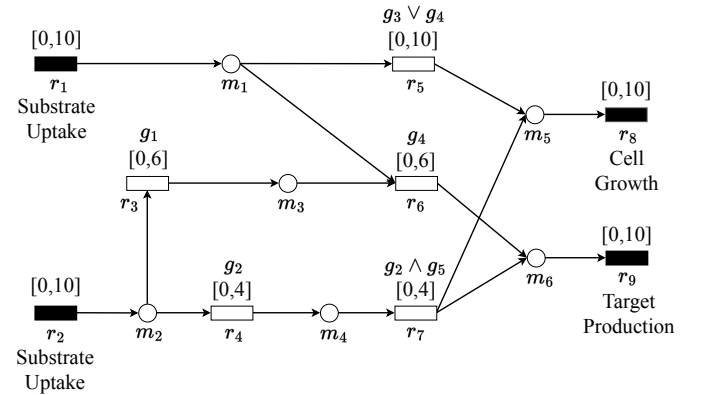


Fig. 1: A toy example of the constraint-based model where circles and rectangles represent metabolites and reactions, respectively. Black and white rectangles denote external and internal reactions, respectively. r_1, r_2 correspond to two substrate uptake reactions. r_8, r_9 correspond to cell growth, and target metabolite production reactions, respectively. The reaction rates are constrained by the range $[l_i, u_i]$. In this example, all stoichiometric ratios are 1 or -1.

$$\begin{aligned}
 & \text{metabolic network part } \mathcal{C}_1, \text{ we have } M = \{m_1, \dots, m_6\}, \\
 & R = \{r_1, \dots, r_9\}, S = \begin{pmatrix} 1 & 0 & 0 & 0 & -1 & -1 & 0 & 0 & 0 \\ 0 & 1 & -1 & -1 & 0 & 0 & 0 & 0 & 0 \\ 0 & 0 & 1 & 0 & 0 & -1 & 0 & 0 & 0 \\ 0 & 0 & 0 & 1 & 0 & 0 & -1 & 0 & 0 \\ 0 & 0 & 0 & 0 & 1 & 0 & 0 & 1 & -1 \\ 0 & 0 & 0 & 0 & 0 & 1 & 1 & 0 & -1 \end{pmatrix}, \\
 & L = \{0, 0, 0, 0, 0, 0, 0, 0, 0\}, \text{ and } U = \{10, 10, 6, 4, 10, 6, 4, 10, 10\}. \text{ For its gene reaction rule part } \mathcal{C}_2, \text{ we have } G = \{g_1, \dots, g_5\},
 \end{aligned}$$

TABLE II: Gene deletion strategies for the toy example in Fig. 1 are classified into five types based on the resulting flux (reaction rate) distributions.

Type	Gene deletion strategies classified by flux distributions
1	$\emptyset, \{g_3\}$
2	$\{g_1\}, \{g_4\}, \{g_1, g_3\}, \{g_1, g_4\}$
3	$\{g_2\}, \{g_5\}, \{g_1, g_2\}, \{g_1, g_5\}, \{g_2, g_3\}, \{g_2, g_4\}, \{g_2, g_5\}, \{g_3, g_5\}, \{g_4, g_5\}, \{g_1, g_2, g_3\}, \{g_1, g_2, g_4\}, \{g_1, g_2, g_5\}, \{g_1, g_3, g_5\}, \{g_1, g_4, g_5\}, \{g_2, g_3, g_5\}, \{g_2, g_4, g_5\}, \{g_1, g_2, g_3, g_5\}, \{g_1, g_2, g_4, g_5\}$
4	$\{g_3, g_4\}, \{g_1, g_3, g_4\}$
5	$\{g_2, g_3, g_4\}, \{g_3, g_4, g_5\}, \{g_1, g_2, g_3, g_4\}, \{g_1, g_3, g_4, g_5\}, \{g_2, g_3, g_4, g_5\}, \{g_1, g_2, g_3, g_4, g_5\}$

TABLE III: The resulting flux distributions for gene deletion strategy Types 1 to 5. For each type, the most optimistic (best) and pessimistic (worst) target metabolite production rate (PR, v_9) at cell growth rate (GR, v_8) maximization are provided.

ID	Deletion strategy	PR situation	Flux distribution								
			v_1	v_2	v_3	v_4	v_5	v_6	v_7	v_8	v_9
1	Type 1	best	10	8	4	4	6	4	4	10	8
		worst	10	0	0	0	10	0	0	0	0
3	Type 2	best	6	4	0	4	6	0	4	10	4
		worst	10	0	0	0	10	0	0	0	0
5	Type 3	best	10	0	0	0	10	0	0	0	0
		worst	10	0	0	0	10	0	0	10	0
7	Type 4	best	0	4	0	4	0	0	4	4	4
		worst	0	4	0	4	0	0	4	4	4
9	Type 5	best	0	0	0	0	0	0	0	0	0
		worst	0	0	0	0	0	0	0	0	0

$F = \{f_1, \dots, f_9\}$, and $P = \{p_1, \dots, p_9\}$, where

$$f_i : p_i = \begin{cases} 1, & i = 1 \\ 1, & i = 2 \\ g_1, & i = 3 \\ g_2, & i = 4 \\ g_3 \vee g_4, & i = 5 \\ g_4, & i = 6 \\ g_2 \wedge g_5, & i = 7 \\ 1, & i = 8 \\ 1, & i = 9 \end{cases}$$

In this toy model \mathcal{C} , because the gene reaction rule of r_7 is given as $f_7 : p_7 = g_2 \wedge g_5$, the reaction rate of r_7 (denoted as v_7) is forced to be 0 if either g_2 or g_5 is 0 (deleted), while if both g_2 and g_5 are 1 (not deleted), then $0 \leq v_7 \leq 4$. However, for r_5 , the reaction rate v_5 is forced to be 0 only if both g_3 and g_4 are 0. However, if at least one of g_3 or g_4 is 1, v_5 can vary within the range $0 \leq v_5 \leq 10$. For r_1, r_2, r_8 , and r_9 , since $p_1 = p_2 = p_8 = p_9 = 1$ always holds, none of v_1, v_2, v_8 , or v_9 can be forced to be 0 by any gene deletions.

In this example, we set m_6 as the target metabolite, produced by the target metabolite production reaction r_9 .

2) **Gene deletions on the toy constraint-based model:** Table II describes the patterns of gene deletions in this example: the $2^5 = 32$ patterns are classified into five types based on the flux distributions. The detailed flux distributions for all types can be found in Table III.

In the original state of the toy model, where no genes are deleted, there are two paths to reach the cell growth reaction r_8 : one begins from the substrate uptake reaction r_1 : ($r_1 \rightarrow r_5 \rightarrow r_8$); the other one begins from the substrate uptake reaction r_2 :

($r_2 \rightarrow r_4 \rightarrow r_7 \rightarrow r_8$). $GR = 10$ can be obtained, but the flux distribution is not uniquely determined.

If both paths are used and the second one ($r_2 \rightarrow r_4 \rightarrow r_7 \rightarrow r_8$) achieves maximum flux, $GR = 10$ and $PR = 8$ can be obtained, as shown in the flux distribution of ID 1 in Table III. This represents the most optimistic case for the value of PR. In contrast, if only the first path ($r_1 \rightarrow r_5 \rightarrow r_8$) is used and achieves maximum flux, then $GR = 10$ and $PR = 0$ are obtained, as shown in the flux distribution of ID 2 in Table III. This represents the most pessimistic case for the value of PR. As previously defined, in the context of growth-coupled production, we need to evaluate the most pessimistic value of PR when GR is maximized. Therefore, in the original state of the toy model, we have $GR = 10$ and $PR = 0$. We denote this flux distribution as Type 1. There is another gene deletion strategy, $\{g_3\}$, which is also classified as Type 1, as it yields the same flux distribution.

IDs 3 and 4 in Table III describe the most optimistic and pessimistic flux distributions with respect to the PR value when g_1 is deleted. When g_1 is deleted, $f_3 : p_3 = g_1 = 0$ is obtained, and v_3 is forced to be zero. The maximum GR is $v_8 = 10$ since both the first and second paths to the growth reaction r_9 (from r_1 or r_2 to r_8) can still be used. In the most optimistic case, both the first path ($r_1 \rightarrow r_5 \rightarrow r_8$) and the second path ($r_2 \rightarrow r_4 \rightarrow r_7 \rightarrow r_8$) are used, with the second one achieving maximum flux; therefore, $GR = 10$ and $PR = 4$ are obtained. In the most pessimistic case, only the first path is used and achieves maximum flux, resulting in $GR = 10$ and $PR = 0$. We denote this flux distribution as Type 2. The gene deletion strategies $\{g_4\}$, $\{g_1, g_3\}$, and $\{g_1, g_4\}$ are also classified as Type 2, as shown in Table III.

IDs 5 and 6 in Table III describe the flux distributions when g_2 is deleted. When g_2 is deleted, $f_4 : p_4 = g_2 = 0$ and $f_7 : p_7 = g_2 \wedge g_5 = 0$ are obtained, forcing v_4 and v_7 to be zero. The maximum GR is $v_8 = 10$ since the first path to the growth reaction (r_1 to r_8) can still be used. This results in a uniquely determined flux distribution where $v_1 = v_5 = 10$ and $v_2 = v_3 = v_4 = v_6 = v_7 = 0$. Consequently, both the optimistic and pessimistic PR values are 0, with GR at 10. We denote this flux distribution as Type 3. Other 17 gene deletion strategies are also classified as Type 3, as shown in Table III.

IDs 7 and 8 in Table III describe the flux distributions when g_3 and g_4 are deleted. When g_3 and g_4 are deleted, $f_5 : p_5 = g_3 \vee g_4 = 0$ and $f_6 : p_6 = g_4 = 0$ are obtained, forcing v_5 and v_6 to be zero. This results in a uniquely determined flux distribution where $v_2 = v_4 = v_7 = 4$ and $v_1 = v_3 = v_5 = v_6 = 0$. Consequently, both the optimistic and pessimistic PR values are 4, with GR also at 4. We denote this flux distribution as Type 4. Another gene deletion strategy $\{g_1, g_3, g_4\}$ is also classified as Type 4, as shown in Table III.

IDs 9 and 10 in Table III describe the flux distributions when g_2, g_3 , and g_4 are deleted. When g_2, g_3 , and g_4 are deleted, $f_4 : p_4 = g_2 = 0$, $f_5 : p_5 = g_3 \vee g_4 = 0$, $f_6 : p_6 = g_4 = 0$, and $f_7 : p_7 = g_2 \wedge g_5 = 0$ are obtained, forcing v_4, v_5, v_6 , and v_7 to be zero. The maximum GR is $v_8 = 0$, as no path to the growth reaction r_8 remains viable. This results in a uniquely determined flux distribution in which all reaction rates are zero, yielding a PR of 0 in both optimistic and pessimistic cases. We denote this flux distribution as Type 5. The gene deletion strategies $\{g_3, g_4, g_5\}$, $\{g_1, g_2, g_3, g_4\}$, $\{g_1, g_3, g_4, g_5\}$, $\{g_2, g_3, g_4, g_5\}$, and $\{g_1, g_2, g_3, g_4, g_5\}$ are also classified as Type 5, as shown in Table III.

Across the five types of gene deletion strategies analyzed, we find that only Type 4 meets the criteria of $PR \geq PR_{\text{threshold}}$

and $GR \geq GR_{\text{threshold}}$, even in the most pessimistic scenarios. Consequently, in our toy model example, only two gene deletion strategies of Type 4, i.e., $\{g_3, g_4\}$ and $\{g_1, g_3, g_4\}$ enable the growth-coupled production of the target metabolite m_6 .

C. Problem Setting

Gene deletion strategy prediction. Given a constraint-based metabolic model \mathcal{C} and a set of metabolites M , the task of gene deletion strategy prediction seeks to infer the gene deletion strategies DS of target metabolites $M_{\text{target}} \subseteq M$. This task operates under the assumption that gene deletion strategies for a subset of metabolites, denoted as DS_{known} , are already established, while the strategies for the target metabolites remain unknown. The primary objective is to develop a computational agent, such as a predictive model $\mathcal{F}(\theta)$, which processes the known deletion strategies along with the information on the metabolic model. This agent aims to generate predictions \tilde{DS} for the target metabolites, optimizing its outputs to closely approximate the ground-truth deletion strategies DS^* , as presented below:

Prediction of Gene Deletion Strategies for Target Metabolites.

Given: $\mathcal{C}, DS_{\text{known}}$

Objective: A computational agent $\mathcal{F}(\theta)$, parameterized by θ , to generate deletion strategy predictions \tilde{DS} for the target metabolites $M_{\text{target}} \subseteq M$.

- 1: **Such that:**
- 2: $\tilde{DS} = \mathcal{F}(\theta; D_{\text{known}}, \mathcal{C});$
- 3: $\tilde{DS} \approx DS^*$

III. METHOD

In this section, we first introduce the overall design and underlying concept of the proposed gene deletion strategy prediction framework. Next, we define each constituent module of the framework and describe the computational model used, illustrating how they perform the gene deletion strategy prediction task. Finally, we provide implementation details, including parameter configurations and model training procedures.

A. Framework Overview

Gene Deletion Strategy Calculation: As previously introduced, the gene deletion strategy calculation is grounded in the constraint-based metabolic model $\mathcal{C} = \{\mathcal{C}_1, \mathcal{C}_2\}$, where $\mathcal{C}_1 = \{M, R, S, L, U\}$ represents metabolite-centric metabolite network, and $\mathcal{C}_2 = \{G, F, P\}$ encompasses gene-related GPR rules. The interactions among metabolites in M and genes in G are modeled in detail, leveraging additional contextual elements from \mathcal{C}_1 and \mathcal{C}_2 , ultimately yielding gene deletion strategies for growth-coupled production. However, the necessary information differs for the gene deletion strategy prediction.

Gene Deletion Strategy Prediction: Specifically, we argue that instead of directly modeling every detailed interaction within the metabolic model, the focus should shift to first capturing the characteristics of metabolites ($M \in \mathcal{C}_1$) and genes ($G \in \mathcal{C}_2$), and then modeling their interdependencies. In this approach, constrained by the observed gene deletion strategies, the detailed interactions among these elements are inferred implicitly rather than explicitly modeled.

In other words, computing gene deletion strategies typically requires a fully parameterized interaction map encompassing

all components in \mathcal{C}_1 and \mathcal{C}_2 . In contrast, given prior knowledge of gene deletion strategies, their prediction necessitates a more targeted approach that prioritizes M and G as the primary sources of information.

Motivated by the above observations, we propose a two-step framework for gene deletion strategy prediction based on metabolite and gene sequential data. This framework is designed to (1) extract the characteristics of metabolites and genes within the metabolic model and (2) model their interdependencies. Specifically, the proposed framework consists of three neural network-based modules to achieve these objectives: the metabolite representation learning module (**Meta-M**), the gene representation learning module (**Gene-M**), and the deletion strategy prediction module (**Pred-M**).

- **Meta-M:** This module captures the characteristics of metabolites within the metabolic model. It formulates a metabolite representation learning task aimed at projecting input metabolite data into a latent representation, Z_{meta} , which summarizes metabolite-relevant information. This unsupervised learning task typically employs a sequential learning model with an autoencoder structure. The learned Z_{meta} serves as the foundation for the downstream gene deletion prediction task.
- **Gene-M:** This module captures the characteristics of genes within the metabolic model. Parallel to Meta-M, it formulates a gene representation learning task aimed at projecting input gene data into a latent representation, Z_{gene} , which summarizes gene-relevant information. Similarly, this unsupervised learning task can also employ a sequential learning model with an autoencoder structure. The learned Z_{gene} serves as the foundation for the downstream gene deletion prediction task.
- **Pred-M:** This module integrates the latent representations Z_{meta} from Meta-M and Z_{gene} from Gene-M into a unified latent representation, Z , capturing the interdependencies between metabolites and genes within the metabolic model. The integration process refines these representations, transforming them into discriminative features optimized for prediction. Finally, a supervised predictor is trained on Z to infer the deletion status of each gene for different target metabolites within the given metabolic model.

B. Gene Deletion Strategy Prediction

1) **Metabolite Representation Learning:** To capture metabolite-specific features, we design Meta-M, utilizing an Long Short-Term Memory (LSTM)-based autoencoder as the backbone neural network model. It is a classic sequential learning model and has been widely used to learn representations from various types of sequential data [29], [30], [31]. We selected LSTM as the default model because our goal is to propose a general framework that enables deep learning in our task setting and to validate its effectiveness. LSTM meets our requirements: it is straightforward to implement and serves as a solid baseline for future comparisons with more complex models, such as Transformer-based architectures [32]. Specifically, Meta-M follows an encoder-decoder architecture, where the encoder network processes the input sequence to capture long-range sequential dependencies and abstract them into latent features. The decoder network then reconstructs the original sequence based on these features.

Given a metabolite sequence input S_m of length L_m , we first tokenize the sequence into a discrete set of tokens and apply

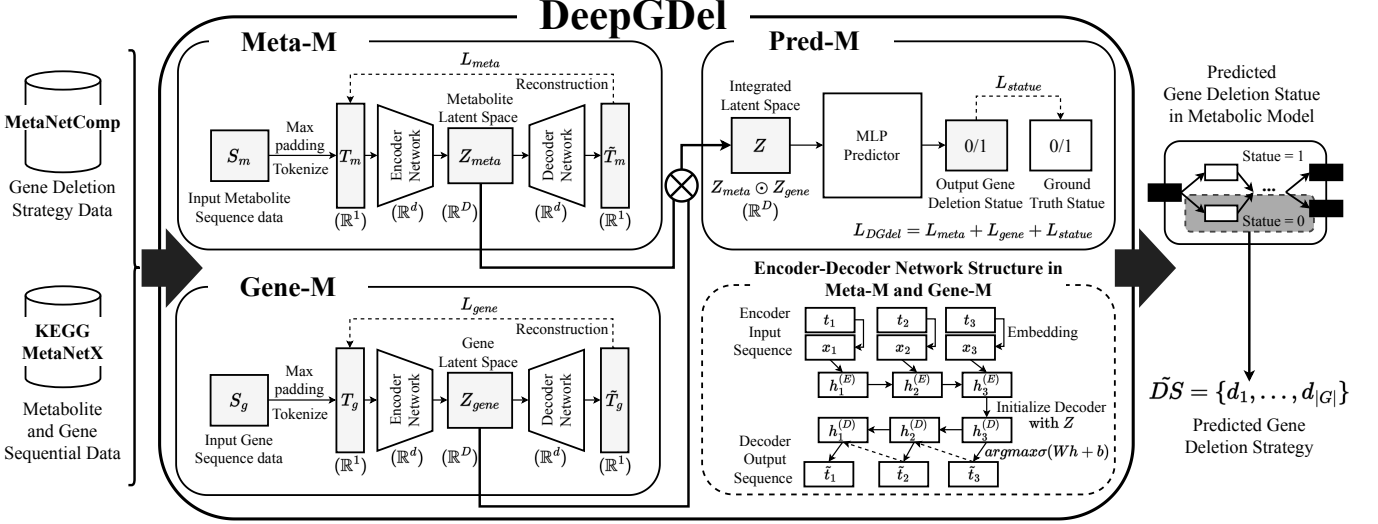


Fig. 2: A system overview of the proposed gene deletion strategy prediction framework.

The framework comprises three neural network-based modules: (1) **Meta-M**, which learns the metabolite latent representation Z_{meta} , (2) **Gene-M**, which learns the gene latent representation Z_{gene} , and (3) **Pred-M**, which integrates the two upstream latents into a new latent representation, Z , for final gene deletion prediction.

padding to ensure all sequences have a uniform length L_{max} . The tokenization step converts the raw metabolite sequence, represented as a string of characters, into a numerical format suitable for processing by the model. Since metabolite sequences consist of characters representing molecular substructures or chemical components, we adopt a character-level tokenization approach. Formally, given a set of N metabolite sequences $\{S_m^{(1)}, S_m^{(2)}, \dots, S_m^{(N)}\}$, we construct a vocabulary \mathcal{V} containing all unique characters appearing in the dataset. Each sequence $S_m^{(i)}$ is then mapped into a sequence of token indices:

$$\mathbf{T}_m^{(i)} = [t_1, t_2, \dots, t_{L_m}], \quad t_j \in \mathcal{V}, \quad (1)$$

where t_j represents the index corresponding to the j -th character in the sequence. To maintain consistency in sequence lengths, we apply max-padding to all tokenized sequences, ensuring they have a uniform length L_{max} :

$$\mathbf{T}_m^{(i)} = [t_1, t_2, \dots, t_{L_m}, 0, 0, \dots, 0], \quad \text{if } L_m < L_{max}. \quad (2)$$

Here, the padding token (denoted as 0) is appended to shorter sequences to match the maximum length found in the training metabolite sequence data. The max-padding ensures that all input sequences share a consistent dimensionality during batch processing. During model training and inference, the model ignores padded positions to prevent them from influencing learned representations.

The padded sequence is then mapped to a continuous embedded representation $\mathbf{X}_m \in \mathbb{R}^d$ via an embedding layer:

$$\mathbf{X}_m = \text{Embedding}(\mathbf{T}_m), \quad (3)$$

where $\text{Embedding}(\cdot)$ denotes a multi-layer perceptron (MLP) transformation. Embedding layers act as a lookup table to perform an implicit one-hot encoding operation. Specifically, given an embedding weight matrix $W_e \in \mathbb{R}^{|\mathcal{V}| \times d}$, the embedding operation can be expressed as:

$$\mathbf{X}_m = W_e[\mathbf{T}_m], \quad (4)$$

where each token index in \mathbf{T}_m selects the corresponding row from W_e , mapping discrete tokens to dense feature vectors. The resulting \mathbf{X}_m captures the high-dimensional feature space of the tokenized input sequence \mathbf{T}_m , representing its categorical characteristics in a continuous embedding space.

The encoder then processes the embedded sequence \mathbf{X}_m through a LSTM network to capture sequential dependencies and compute the hidden states \mathbf{h}_l at each time step l :

$$\mathbf{h}_l = \text{LSTM-Encoder}(\mathbf{X}_m, \mathbf{h}_{l-1}), \quad (5)$$

where $\mathbf{h}_l \in \mathbb{R}^D$ represents the hidden state at time step l , and \mathbf{h}_0 denotes the initial hidden state.

The LSTM-Encoder consists of a recurrent structure encodes the long-range contextual information and preserve key features across the metabolic sequence into these hidden states. Specifically, following the definitions in [33], at each time step l , the LSTM cell updates its hidden state \mathbf{h}_l and cell state \mathbf{c}_l based on the input embedding \mathbf{x}_l and the previous states $(\mathbf{h}_{l-1}, \mathbf{c}_{l-1})$:

$$\mathbf{i}_l = \sigma(\mathbf{W}_i \mathbf{x}_l + \mathbf{U}_i \mathbf{h}_{l-1} + \mathbf{b}_i), \quad (6)$$

$$\mathbf{f}_l = \sigma(\mathbf{W}_f \mathbf{x}_l + \mathbf{U}_f \mathbf{h}_{l-1} + \mathbf{b}_f), \quad (7)$$

$$\mathbf{o}_l = \sigma(\mathbf{W}_o \mathbf{x}_l + \mathbf{U}_o \mathbf{h}_{l-1} + \mathbf{b}_o), \quad (8)$$

$$\tilde{\mathbf{c}}_l = \tanh(\mathbf{W}_c \mathbf{x}_l + \mathbf{U}_c \mathbf{h}_{l-1} + \mathbf{b}_c), \quad (9)$$

$$\mathbf{c}_l = \mathbf{f}_l \odot \mathbf{c}_{l-1} + \mathbf{i}_l \odot \tilde{\mathbf{c}}_l, \quad (10)$$

$$\mathbf{h}_l = \mathbf{o}_l \odot \tanh(\mathbf{c}_l), \quad (11)$$

where \mathbf{i}_l , \mathbf{f}_l , and \mathbf{o}_l denote the input, forget, and output gates, respectively. The cell state \mathbf{c}_l stores long-term memory, and $\tilde{\mathbf{c}}_l$ represents the candidate cell state. The weight matrices and bias terms have the following dimensions:

$$\mathbf{W}_i, \mathbf{W}_f, \mathbf{W}_o, \mathbf{W}_c \in \mathbb{R}^{D \times d},$$

$$\mathbf{U}_i, \mathbf{U}_f, \mathbf{U}_o, \mathbf{U}_c \in \mathbb{R}^{D \times D},$$

$$\mathbf{b}_i, \mathbf{b}_f, \mathbf{b}_o, \mathbf{b}_c \in \mathbb{R}^D,$$

where \mathbf{W}_* transforms the input embedding $\mathbf{x}_l \in \mathbb{R}^d$, \mathbf{U}_* transforms the previous hidden state $\mathbf{h}_{l-1} \in \mathbb{R}^D$, and \mathbf{b}_* are bias terms. The operator \odot denotes element-wise multiplication, while $\sigma(\cdot)$ and $\tanh(\cdot)$ represent the sigmoid and hyperbolic tangent activation functions, respectively.

Subsequently, we apply layer normalization to the LSTM outputs:

$$\mathbf{h}_l^{\text{norm}} = \text{LayerNorm}(\mathbf{h}_l), \quad (12)$$

where $\text{LayerNorm}(\cdot)$ represents the layer normalization operation, and $\mathbf{h}_l^{\text{norm}} \in \mathbb{R}^D$ denotes the normalized hidden state at time step l . This normalization step mitigates internal covariate shift by normalizing the hidden states across features, thereby enhancing both training stability and the model's generalization capacity.

The final latent representation \mathbf{Z}_{meta} produced by the encoder of Meta-M is obtained by applying average pooling over the sequence of normalized hidden states:

$$\mathbf{Z}_{\text{meta}} = \text{AvgPooling}(\{\mathbf{h}_l^{\text{norm}}\}_{l=1}^{L_m}), \quad (13)$$

where $\text{AvgPooling}(\cdot)$ performs average pooling across the sequence of normalized hidden states, producing a single vector representation $\mathbf{Z}_{\text{meta}} \in \mathbb{R}^D$. This pooling operation aggregates information across the entire sequence in a stable manner, providing a global summary of the metabolite's features.

The decoder decodes the hidden state \mathbf{h}_l at each time step from the latent representation \mathbf{Z}_{meta} :

$$\mathbf{h}_l = \text{LSTM-Decoder}(\mathbf{Z}_{\text{meta}}, \mathbf{h}_{l-1}), \quad (14)$$

where the LSTM-Decoder follows a similar LSTM-based computation as described in Equation (6) to (11), but in reverse, using the hidden states \mathbf{h}_l and cell states \mathbf{c}_l to generate a sequence of hidden state. The decoder is initialized using \mathbf{Z}_{meta} , which serves as the initial hidden and cell states:

$$\mathbf{h}_0 = \mathbf{W}_h \mathbf{Z}_{\text{meta}} + \mathbf{b}_h, \quad \mathbf{c}_0 = \mathbf{W}_c \mathbf{Z}_{\text{meta}} + \mathbf{b}_c. \quad (15)$$

The final output of the generated tokenized sequence $\tilde{\mathbf{T}}_m$ is given through:

$$\tilde{\mathbf{T}}_m = \text{GenerateToken}(\mathbf{h}_l), \quad (16)$$

where $\text{GenerateToken}(\cdot)$ represents a projection layer followed by a softmax function to generate $\tilde{\mathbf{t}}_l$, corresponding to each character in the tokenized sequence:

$$\tilde{\mathbf{t}}_l = \arg \max \sigma(\mathbf{W}_{\text{out}} \mathbf{h}_l + \mathbf{b}_{\text{out}}), \quad (17)$$

where $\sigma(\cdot)$ denotes the softmax activation function, and \mathbf{W}_{out} and \mathbf{b}_{out} are the weights and bias of the output projection layer.

The training of the Meta-M encoder-decoder network is performed by minimizing the categorical cross-entropy loss during tokenized input metabolite sequence reconstruction. The objective function is defined as:

$$\mathcal{L}_{\text{meta}} = \frac{1}{L_m} \sum_{l=1}^{L_m} \text{CrossEntropyLoss}(\tilde{\mathbf{t}}_l, \mathbf{t}_l), \quad (18)$$

where \mathbf{t}_l and $\tilde{\mathbf{t}}_l$ represent the ground-truth token and predicted logits at time step l , respectively. The categorical cross-entropy loss for each token is given by:

$$\text{CrossEntropyLoss}(\tilde{\mathbf{t}}_l, \mathbf{t}_l) = - \sum_{i=1}^C t_{l,i} \log \tilde{t}_{l,i}, \quad (19)$$

where C denotes the vocabulary size, $t_{l,i}$ represents the one-

hot encoded ground-truth distribution, and $\tilde{t}_{l,i}$ is the predicted probability of token i at position l .

The cross-entropy loss quantifies the dissimilarity between the predicted and true probability distributions. It penalizes the model more heavily when incorrect predictions receive higher probabilities, thereby encouraging the model to produce a probability distribution that closely aligns with the true distribution. By minimizing this loss, Meta-M learns to encode the input metabolite sequence into \mathbf{Z}_{meta} and leverage it to reconstruct the sequence with high fidelity. As a result, \mathbf{Z}_{meta} serves as a compact and informative representation of the metabolite sequence, capturing its essential features.

2) *Gene Representation Learning*: To capture gene-specific features, we design Gene-M, an encoder-decoder module parallel to Meta-M, using the same LSTM structure but applied to gene sequence data. This parallel architecture ensures that both input types—gene and metabolite sequences—are processed equally, without bias, within a unified framework. Specifically, similar to Meta-M, Gene-M learns gene representations by reconstructing the original gene sequence.

Given a gene sequence input \mathbf{S}_g of length L_g , after the aforementioned tokenize and padding operations, we obtain \mathbf{T}_g . Gene-M processes its reconstruction through the following network architecture:

$$\left\{ \begin{array}{l} \mathbf{X}_g = \text{Embedding}(\mathbf{T}_g), \\ \mathbf{h}_l = \text{LSTM-Encoder}(\mathbf{X}_g, \mathbf{h}_{l-1}), \\ \mathbf{h}_l^{\text{norm}} = \text{LayerNorm}(\mathbf{h}_l), \\ \mathbf{Z}_{\text{gene}} = \text{AvgPooling}(\{\mathbf{h}_l^{\text{norm}}\}_{l=1}^{L_g}), \\ \mathbf{h}_l = \text{LSTM-Decoder}(\mathbf{Z}_{\text{gene}}, \mathbf{h}_{l-1}), \\ \tilde{\mathbf{T}}_g = \text{GenerateToken}(\mathbf{h}_l), \end{array} \right. \quad (20)$$

where $\mathbf{X}_g \in \mathbb{R}^d$ denotes the continuous embedded representation of \mathbf{T}_g , $\mathbf{Z}_{\text{gene}} \in \mathbb{R}^D$ denotes the final gene latent representation, and $\tilde{\mathbf{T}}_g$ denotes the reconstructed original tokenized gene sequence.

The training of the Gene-M encoder-decoder network is performed by minimizing the categorical cross-entropy loss during gene sequence reconstruction. The objective function is defined as:

$$\mathcal{L}_{\text{gene}} = \frac{1}{L_g} \sum_{l=1}^{L_g} \text{CrossEntropyLoss}(\tilde{\mathbf{t}}_l, \mathbf{t}_l), \quad (21)$$

where \mathbf{t}_l and $\tilde{\mathbf{t}}_l$ represent the ground-truth token and predicted logits at time step l , respectively. By minimizing this loss, Gene-M learns to encode the input gene sequence into \mathbf{Z}_{gene} and leverage it to reconstruct the sequence with high fidelity. As a result, \mathbf{Z}_{gene} serves as a compact and informative representation of the gene sequence, capturing its essential features.

3) *Gene Deletion Status Prediction*: The Pred-M module integrates the learned representations \mathbf{Z}_{meta} and \mathbf{Z}_{gene} using element-wise multiplication:

$$\mathbf{Z} = \mathbf{Z}_{\text{meta}} \odot \mathbf{Z}_{\text{gene}}. \quad (22)$$

In this context, \mathbf{Z}_{meta} and \mathbf{Z}_{gene} are the learned representations of the metabolite and gene sequences, respectively, both residing in the same D -dimensional feature space. The resulting vector $\mathbf{Z} \in \mathbb{R}^D$ combines the gene and metabolite information by multiplying the corresponding entries of \mathbf{Z}_{meta} and \mathbf{Z}_{gene} at each dimension. The element-wise multiplication serves to emphasize the dimensions where both representations align,

TABLE IV: Grid search for hyperparameter selection. The optimal values are highlighted in underline.

Hyperparameter	Search Space
Embedding dimension (\mathbb{R}^d)	{16, <u>32</u> , 64, 128}
LSTM hidden state	{16, 32, <u>64</u> , 128}
Embedding dimension (\mathbb{R}^D)	{16, 32, <u>64</u> , 128}
Dropout rate	{0, 0.1, 0.2}
Batch size	{ <u>8</u> , 16, 32, 64}

while reducing the impact of less significant features. The final vector \mathbf{Z} serves as a compact, interaction-based representation that incorporates both individual and combined features from the gene and metabolite sequences.

A supervised predictor of Pred-M uses \mathbf{Z} as input and outputs the gene deletion status as a binary classification within a given metabolic model:

$$\hat{y} = \sigma(\text{MLP}(\mathbf{Z})), \quad (23)$$

where $\sigma(\cdot)$ is the sigmoid activation function. The loss function for the deletion status classification task, $\mathcal{L}_{\text{status}}$, is the binary cross-entropy loss:

$$\mathcal{L}_{\text{status}} = - \sum_i \left(y_i \log \hat{y}_i + (1 - y_i) \log (1 - \hat{y}_i) \right), \quad (24)$$

where y_i is the true label and \hat{y}_i is the predicted probability.

The final loss function of the proposed gene deletion strategy prediction framework combines the reconstruction losses from the two representation learning tasks of Meta-M and Gene-M, along with the binary gene deletion status classification task:

$$\mathcal{L}_{\text{DBgDel}} = \mathcal{L}_{\text{meta}} + \mathcal{L}_{\text{gene}} + \mathcal{L}_{\text{pred}}. \quad (25)$$

C. Implementation Details and Model Training

1) *Device*: All neural network models were trained within the proposed framework on an NVIDIA A100-PCIE-40GB GPU with a Xeon Gold 6258R CPU. Model parameters were optimized for 100 epochs using the Adam optimizer with a learning rate of 1×10^{-3} .

2) *Data Splitting and Balancing*: We employed a 10-fold stratified cross-validation scheme, repeated five times with different random seeds. In each fold, approximately 10% of metabolites were reserved for testing, while the remainder formed the training set. From the training data, 10% of metabolites were randomly selected as a validation set. To ensure balanced proportions of deleted and non-deleted genes across training, validation, and test sets, we applied a gene-wise balancing procedure: for genes with both deletion states, equal samples were randomly drawn from each state; otherwise, all instances were retained. Next, global class balancing was performed by downsampling the majority class to match the minority, yielding a fully balanced training set. Due to metabolite number constraints, final sample sizes may only approximate the intended ratios. Performance metrics are reported as mean and standard deviation across all folds.

3) *Hyperparameters*: The hyperparameters of the neural network models were determined via grid search to identify the optimal configuration, as summarized in Table IV. The selected values were adopted as the default settings for the proposed framework.

TABLE V: Mathematical notations and their explanations in the computational experiments section.

Notation	Description
$N_0(g, m)$	Deleted occurrences for gene g in metabolite m
$N_1(g, m)$	Non-deleted occurrences for gene g in metabolite m
$N_{\text{total}}(g)$	Total occurrences for gene g across all metabolites
$q_1(g)$	Proportion of non-deleted occurrences for gene g
$\hat{y}(g)$	Prediction for gene g (non-deleted or deleted)
y_{pred}	Final prediction array for all genes
TP_{m_i}	True positives for class i ($i = 0$ or 1) in metabolite m
FP_{m_i}	False positives for class i ($i = 0$ or 1) in metabolite m
TN_{m_i}	True negatives for class i ($i = 0$ or 1) in metabolite m
FN_{m_i}	False negatives for class i ($i = 0$ or 1) in metabolite m

4) *Computational Complexity and Runtime*: The proposed framework adopts an LSTM-based autoencoder as the backbone neural network model. The computational complexity of a single LSTM layer is approximately $\mathcal{O}(L \cdot d \cdot h)$, where L is the sequence length, d is the input embedding size, and h is the number of hidden units. The proposed framework incorporates two LSTM models in both Meta-M and Gene-M. Consequently, the per-step framework complexity is dominated by the terms $\mathcal{O}(c \cdot L \cdot d \cdot h)$, where the factor c arises from the LSTM layer size in the encoder and decoder.

For model training with a batch size of B , the overall computational complexity for parallel processing the input gene sequences of length L_g and metabolite sequences of length L_s is $\mathcal{O}(B \cdot (L_g + L_s) \cdot c \cdot d \cdot h)$. The sequence lengths L_g and L_s are the dominant factors influencing the time complexity, as they are fixed by the input and directly affect the per-step computations. The actual time cost also depends on setting the number of hidden units, embedding size, and layer size, as all these hyperparameters of the neural network contribute to the overall computational demand. Empirically, the framework, following the optimal values in Table IV, demonstrates efficient training, completing 100 epochs in approximately 10 hours under our experimental conditions.

IV. COMPUTATIONAL EXPERIMENTS

In this section, we first provide an overview of our design for computational experiments on metabolic models. Next, we describe the experimental setup in detail, including the data, baseline methods, and evaluation metrics employed. Finally, we present the experimental results along with key observations. All the notations mentioned in this section are listed in Table V.

A. Overview

In the computational experiments, we consider three metabolic models: *e_coli_core*, *iMM904*, and *iML1515*:

- *e_coli_core* [34] is a simplified metabolic model of *Escherichia coli* (E. coli) that captures only the essential pathways necessary for core metabolic functions. It is widely used for foundational studies of bacterial metabolism and gene interactions.
- *iMM904* [35] is a more comprehensive model of *Saccharomyces cerevisiae* (yeast), incorporating a larger set of reactions and metabolites. It is commonly used for analyzing complex eukaryotic metabolic networks.
- *iML1515* [36] is one of the most detailed metabolic models of E. coli, covering a vast array of metabolic reactions and

TABLE VI: Summary of constraint-based metabolic models used in the computational experiment.

Metabolic model	<i>e_coli_core</i>	<i>iMM904</i>	<i>iML1515</i>
#Genes	137	905	1516
#Growth essential genes	7	110	196
#Pre-determined genes	71	850	1483
#Metabolites	72	1226	1877
#GCP-possible metabolites	48	782	1085
#Reactions	95	1577	2712

pathways. It provides a more intricate network compared to *e_coli_core* and is widely used as a genome-scale model for simulations.

We further define several key terms employed in our computational experiments as follows:

- **Growth-essential genes:** These are genes whose deletion results in a maximum GR of zero during FBA. They are crucial for cell growth and should not be deleted when aiming for growth-coupled production.
- **Pre-determined genes:** A gene is defined as pre-determined if its deletion state is consistent (either fully deleted or fully non-deleted) for more than 95% of metabolites within the metabolic model. Such genes' deletion states are considered stable and will not be included in the prediction evaluation.
- **GCP-possible metabolites:** These metabolites are theoretically capable of achieving growth-coupled production within the metabolic models. Only GCP-possible metabolites are considered suitable for targeting when calculating gene deletion strategies.

The quantitative breakdown of genes, metabolites, and reactions in these models is summarized in Table VI.

To explore the feasibility of applying gene deletion prediction models to the aforementioned metabolic models, we design two computational experiments as follows:

- 1) Evaluate the performance of gene deletion prediction methods, including the proposed framework and baseline methods. Both methods are applied to three metabolic models, and the results for each model are compared individually.
- 2) Investigate the impact of different input data types on the performance of the proposed framework. An ablation study is conducted, where the proposed framework is trained using only one type of input data (either sequential data on gene or metabolite). The results of the two ablation variants are applied to three metabolic models, and the results for each model are compared individually.

B. Data and Preprocessing

For the experiments, we use data from three categories: (1) gene deletion strategy data, which serves as the ground truth for prediction tasks; (2) SMILES data, which provides information on the metabolites in the metabolic models; and (3) amino acid (AA) sequence data, which provides information on the genes, specifically their encoded proteins in the metabolic models. The details of the constructed datasets are summarized in Table VII.

1) **Gene Deletion Strategy Data: Description.** In this study, we preserve gene deletion strategy data in the form of binary sequences to record the deletion strategies for specific

TABLE VII: Summary of constructed datasets for three constraint-based metabolic models.

Metabolic model	<i>e_coli_core</i>	<i>iMM904</i>	<i>iML1515</i>
#Deletion strategies	41	105	443
#Genes per strategy	137	905	1516
#SMILES terms	41	99	425
#Dummy SMILES terms	0	6	18
#AA Seq. terms	136	889	1513
#Dummy AA Seq. terms	1	16	3
#Balanced train/val samples	4932	85070	603368
#Balanced test samples	685	9955	68220

metabolites. Specifically, the gene deletion strategy data $DS = (d_1, \dots, d_{|G|})$ represents a binary sequence of length $|G|$, where $|G|$ is the number of genes in the metabolic model, and each element $d_i \in \{0, 1\}$ corresponds to the state of gene i : $d_i = 0$ if gene i is deleted and $d_i = 1$ if it is non-deleted.

A single target metabolite may have multiple deletion strategies, indicating that more than one strategy can lead to the growth-coupled production of that metabolite. This study focuses on the maximal gene deletion strategy data based on the available strategies in the database, denoted as DS_{\max} , where deleting one more gene will result in the loss of growth-coupled production achievement.

Data Source. The gene deletion strategy data used in this study is obtained from the MetNetComp database [19]. MetNetComp is a web-based database system that provides simulation-based gene deletion strategies for achieving growth-coupled production in constraint-based metabolic networks. It curates data from systematically simulated results obtained through constraint-based models. MetNetComp computed growth-coupled gene deletion strategies that are minimal or maximal regarding the number of gene deletions by modifying strategies given by the gDel_minRN algorithm. To date, MetNetComp features an extensive repository of 85,611 gene deletion strategies for 1,735 target metabolites across ten species.

We download all available maximal gene deletion strategy data for the three metabolic models under study: *e_coli_core*, *iMM904*, and *iML1515* from the MetNetComp database. The raw data comprises four categories of information: (1) the number of remaining genes, (2) the maximum growth rate, (3) the minimum production rate, and (4) a list of remaining genes. We use only the list in (4), which specifies the genes that are non-deleted in the maximal gene deletion strategy. The gene deletion strategy data of binary sequence can be easily derived from this information.

2) **SMILES Data: Description.** The SMILES (Simplified Molecular Input Line Entry System) data represents the metabolites used in the studied metabolic models. It presents the chemical structures of metabolites as string representations. Each SMILES string encodes a metabolite molecule's structure, including atoms, bonds, and stereochemistry, in a textual format composed of characters, including alpha letters and notations. SMILES data has become one of the most well-used formats in analyzing compound chemical properties, such as molecular similarity, substructure searches, and cheminformatics-driven predictions. For broader calculation needs, SMILES data are commonly transformed into other data formats, such as molecule fingerprints of binary sequences.

Data Source. The SMILES data used in this study is ob-

tained from the MetaNetX database. MetaNetX is an online platform for accessing, analyzing, and manipulating genome-scale metabolic networks and biochemical pathways. It curates information from public repositories to integrate data on metabolites and related reactions across species.

For all three metabolic models under study, we download the SMILES data for metabolites from the MetaNetX database, corresponding to those for which gene deletion strategy data is available. We employ dummy SMILES sequences as placeholders for metabolites that lacked corresponding SMILES data in the database.

3) **Amino Acid Sequence Data: Description.** Since in metabolic models, the gene function reflected by the GPR rule is ultimately carried out by the encoded protein, we use the amino acid (AA) sequence as the source of gene information. The AA sequence represents each protein corresponding to the genes in the metabolic models as a linear sequence of amino acids, using the standard one-letter amino acid codes—a set of 20 characters in string format. AA sequence data has been widely used to study protein structures and functions, including protein functional annotation, structural prediction, and the investigation of protein-protein interactions.

Data Source. The AA sequence data used in this study is obtained from the KEGG (Kyoto Encyclopedia of Genes and Genomes) database. KEGG provides comprehensive information on protein-coding genes, their products, and associated metabolic pathways. The AA sequence data in KEGG is curated from publicly available genomic resources and is continuously updated to ensure accuracy and relevance.

We download the AA sequence data for all three metabolic models under study from the KEGG database, corresponding to all the genes in each model. We employ dummy AA sequence sequences as placeholders for genes that lacked corresponding AA sequence data in the database.

C. Baseline Method: BPM

1) **Definition:** We employ a Baseline Prediction Method (BPM) based on a proportion and thresholding approach in the experiment. This baseline method classifies gene deletion states as follows:

Given a gene $g \in G$, let $N_0(g, m)$ be the number of deleted occurrences and $N_1(g, m)$ the number of non-deleted occurrences for g across all metabolites m in the training set. The total number of occurrences for g in the training set is:

$$N_{total}(g) = \sum_{m \in M} [N_0(g, m) + N_1(g, m)]$$

The proportion of non-deleted occurrences $q_1(g)$ is then given by:

$$q_1(g) = \frac{\sum_M N_1(g, m)}{\sum_M [N_0(g, m) + N_1(g, m)]}$$

The baseline prediction $\hat{y}(g)$ for g is determined by comparing $q_1(g)$ to a threshold ratio τ . This prediction can be formulated as:

$$\hat{y}(g) = \begin{cases} 1, & \text{if } q_1(g) > \tau \\ 0, & \text{otherwise} \end{cases}$$

where $\hat{y}(g) = 1$ indicates that the gene is predicted as non-deleted, and $\hat{y}(g) = 0$ indicates that the gene is predicted as deleted. The model is trained on datasets balanced by deletion statuses and we choose $\tau = 0.5$ as the default setting to balance sensitivity and specificity.

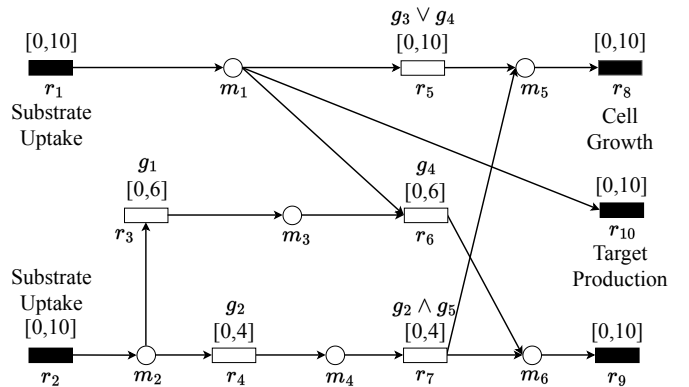


Fig. 3: The toy model with a new target metabolite. Black rectangles denote external reactions. r_1, r_2 correspond to two substrate uptake reactions. r_8, r_{10} correspond to cell growth, and target metabolite production reactions, respectively.

The final prediction array y_{pred} is constructed by applying this formula across all genes g_i in the dataset:

$$y_{pred} = [\hat{y}(g_1), \hat{y}(g_2), \dots, \hat{y}(g_{|G|})]$$

The above baseline method involves calculating proportions and a threshold-based decision-making process. This simplicity makes it a reference point for understanding how more complex models perform in comparison to a straightforward rule.

2) **Example:** We apply the BPM method to the previously constructed toy model with a new target metabolite to demonstrate its execution in the gene deletion strategy prediction task. As shown in Fig. 3, the new target metabolite is set as m_1 . In the original model, m_1 does not have an associated external reaction. Therefore, it is necessary to introduce an auxiliary reaction, r_{10} , to simulate the secretion of m_1 . The configurations of the \mathcal{C}_1 and \mathcal{C}_2 parts of the toy model remain unchanged from the original settings described in Section II-B1. The gene deletion strategies for m_6 described in Section II-B2 are used as the training data.

Step 1: Extract Training Data. In this example, the training dataset contains only one maximal gene deletion strategy $D_{\max} = \{g_1, g_3, g_4\}$ (i.e., the gene deletion of Type 4 in Table II) for another metabolite, m_6 . This set specifies that g_2 and g_5 are essential genes for achieving GCP of m_6 .

Step 2: Compute Occurrence Counts. For each gene g_i in the toy model, referring D_{\max} , the counts are derived as follows:

$$N_0(g_i, m_6) = 1, N_1(g_i, m_6) = 0 \quad \text{for } g_i \in \{g_1, g_3, g_4\},$$

$$N_0(g_i, m_6) = 0, N_1(g_i, m_6) = 1 \quad \text{for } g_i \in \{g_2, g_5\}.$$

Step 3: Calculate Non-Deleted Proportions. The proportion of non-deleted occurrences $q_1(g_i)$ for each gene is calculated as follows:

$$q_1(g_i) = \frac{N_1(g_i)}{N_0(g_i) + N_1(g_i)} = \begin{cases} 0, & i = 1 \\ 1, & i = 2 \\ 0, & i = 3 \\ 0, & i = 4 \\ 1, & i = 5 \end{cases}$$

Step 4: Apply Threshold to Predict States. Using the

threshold $\tau = 0.5$, the state of each gene g_i is predicted as:

$$\begin{aligned} g_1 : q_1(g_1) &= 0.0 < 0.5 \Rightarrow \hat{y}(g_1) = 0, \\ g_2 : q_1(g_2) &= 1.0 > 0.5 \Rightarrow \hat{y}(g_2) = 1, \\ g_3 : q_1(g_3) &= 0.0 < 0.5 \Rightarrow \hat{y}(g_3) = 0, \\ g_4 : q_1(g_4) &= 0.0 < 0.5 \Rightarrow \hat{y}(g_4) = 0, \\ g_5 : q_1(g_5) &= 1.0 > 0.5 \Rightarrow \hat{y}(g_5) = 1. \end{aligned}$$

As a result, in this example, the BPM method predicts the gene deletion strategy for m_1 in the toy model as follows:

$$y_{pred} = [0, 1, 0, 0, 1]$$

This indicates that the states of gene g_1 , g_3 , and g_4 are deleted, while g_2 and g_5 remain non-deleted.

D. Baseline Method: DNN

1) **Definition:** Besides the BPM, which serves as a null-model baseline, we also employ a deep learning-based baseline: a Deep Neural Network (DNN) [37] for the prediction of gene deletion status. DNNs are widely used as standard baselines in supervised learning tasks due to their ability to capture non-linear relationships in high-dimensional data, even with simple model structures.

In our case, the DNN baseline takes as input the same tokenized and padded sequences of the gene T_g and the metabolite T_m as used in our proposed framework. In contrast to the modular, task-specific architecture of our method, this baseline adopts a simplified design: T_g and T_m are independently mapped to dense vectors via separate embedding layers and then concatenated to form a joint representation:

$$\begin{aligned} \mathbf{X}_g &= \text{Embedding}(\mathbf{T}_g), \\ \mathbf{X}_m &= \text{Embedding}(\mathbf{T}_m), \\ \mathbf{X} &= [\mathbf{X}_g; \mathbf{X}_m]. \end{aligned}$$

The resulting concatenated embedding \mathbf{X} is then passed through two fully connected layers with ReLU activations, followed by a sigmoid output layer that produces a probability score:

$$\begin{cases} \mathbf{h}_1 = \text{ReLU}(\mathbf{W}_1 \mathbf{X} + \mathbf{b}_1), \\ \hat{y} = \sigma(\mathbf{W}_2 \mathbf{h}_1 + \mathbf{b}_2), \end{cases} \quad (26)$$

where $\hat{y} = P(y = 1 \mid \mathbf{T}_g, \mathbf{T}_m; \theta)$, $y \in \{0, 1\}$ denotes the ground-truth label (deleted or non-deleted), and $\theta = \{\mathbf{W}_1, \mathbf{W}_2, \mathbf{b}_1, \mathbf{b}_2\}$ represents the set of learnable parameters.

The DNN is trained using the same training setup as the proposed framework and the binary cross-entropy loss as training objective, as defined in Equation (24).

This DNN baseline provides a point of comparison for a naive learnable classifier that does not incorporate any task-specific design. Its performance helps evaluate the necessity of our proposed modular design, which integrates distinct tasks (i.e., representation learning in Gene-M and Meta-M) within the framework.

E. Evaluation Metrics

Our experiments use four evaluation metrics: overall accuracy, macro-averaged precision, recall, and F1 score. Their definitions are provided below.

Overall Accuracy: Accuracy measures the proportion of correctly classified instances out of the total instances. In our experiments, overall accuracy represents the proportion of

genes correctly classified as deleted or non-deleted across all metabolites. It is given by:

$$\text{Overall Accuracy} = \frac{\sum_{m=1}^{|M|} \sum_{i=0}^1 (TP_{mi} + TN_{mi})}{|M| \times |G|}$$

Macro-Averaged Precision: Precision measures the proportion of true positive predictions out of all positive predictions for each class. The macro-averaged precision is the average of precision values across both classes (deleted and non-deleted genes) and is calculated as:

$$\text{Macro-Averaged Precision} = \frac{1}{|M|} \sum_{m=1}^{|M|} \frac{1}{2} \sum_{i=0}^1 \frac{TP_{mi}}{TP_{mi} + FP_{mi}}$$

Macro-Averaged Recall: Recall (or sensitivity) measures the proportion of true positives out of all actual positives for each class. The macro-averaged recall is the average of recall values across both classes and is given by:

$$\text{Macro-Averaged Recall} = \frac{1}{|M|} \sum_{m=1}^{|M|} \frac{1}{2} \sum_{i=0}^1 \frac{TP_{mi}}{TP_{mi} + FN_{mi}}$$

Macro-Averaged F1 Score: The F1 score is the harmonic mean of precision and recall for each class. The macro-averaged F1 score is the average of F1 scores across both classes and is given by:

$$\text{Macro-Averaged F1 Score} = \frac{1}{|M|} \sum_{m=1}^{|M|} \frac{1}{2} \sum_{i=0}^1 2 \cdot \frac{\text{Prec.}_m \cdot \text{Recall}_m}{\text{Prec.}_m + \text{Recall}_m}$$

Macro-Averaged AUC: The Area Under the Receiver Operating Characteristic Curve (AUC) quantifies the ability of a model to discriminate between the two classes. For each metabolite m , the AUC is computed based on the predicted scores and true labels. It is given by:

$$\text{AUC}_m = \frac{1}{|P_m| |N_m|} \sum_{p \in P_m} \sum_{n \in N_m} \left[\mathbb{I}(s_p > s_n) + \frac{1}{2} \mathbb{I}(s_p = s_n) \right],$$

where P_m and N_m are the sets of indices of positive (deleted) and negative (non-deleted) genes for metabolite m , s_p and s_n are the predicted scores (probabilities) for gene p and n , respectively, $\mathbb{I}(\cdot)$ is the indicator function that returns 1 if the condition holds, and 0 otherwise. The macro-averaged AUC is the average of the AUC scores across all metabolites:

$$\text{Macro-Averaged AUC} = \frac{1}{|M|} \sum_{m=1}^{|M|} \text{AUC}_m$$

F. Results and Performance Comparison

The results of two computational experiments—(1) performance comparisons with baseline methods and (2) ablation tests on input data type—across the three metabolic models under study are summarized in Table VIII and Table IX, respectively.

For *e_coli_core*: Table VIII item '*e_coli_core*' summarizes the performance comparison between the proposed framework DBgDel and baseline methods in the context of targeting GCP-possible metabolites of *e_coli_core* metabolic model. Regarding overall accuracy, DBgDel achieved the highest score of 74.85% across all tested target metabolites. In comparison, the BPM and DNN baselines achieved 57.21% and 62.68%, respectively. Regarding the macro-averaged precision, recall,

TABLE VIII: Comparison of gene deletion strategy prediction performance between the proposed DeepGDel framework and two baseline methods across the three metabolic models under study. “M-Avg.” stands for Macro-averaged. The best-performing results are highlighted in bold.

Metric	e_coli_core			iMM904			iML1515		
	BPM	DNN	Proposed	BPM	DNN	Proposed	BPM	DNN	Proposed
Overall Accuracy (%)	57.21 \pm 5.17	62.68 \pm 2.67	71.90 \pm 0.45	57.27 \pm 7.89	69.98 \pm 1.57	79.78 \pm 0.44	54.21 \pm 1.82	60.44 \pm 1.03	67.24 \pm 0.34
M-Avg. Precision (%)	56.68 \pm 5.83	64.35 \pm 2.54	71.72 \pm 0.55	54.38 \pm 7.62	72.48 \pm 1.46	78.29 \pm 0.42	54.04 \pm 2.61	63.96 \pm 1.12	69.59 \pm 0.36
M-Avg. Recall (%)	71.04 \pm 13.87	64.78 \pm 2.22	72.15 \pm 0.53	73.29 \pm 13.79	67.84 \pm 1.38	77.08 \pm 0.44	60.03 \pm 12.89	62.09 \pm 1.10	63.76 \pm 0.34
M-Avg. F1 Score (%)	61.35 \pm 7.63	60.19 \pm 2.38	70.14 \pm 0.64	60.00 \pm 7.28	64.20 \pm 1.54	77.25 \pm 0.45	55.15 \pm 5.65	58.11 \pm 1.16	62.59 \pm 0.34
M-Avg. AUC (%)	56.74 \pm 8.29	62.04 \pm 2.86	71.88 \pm 0.86	53.06 \pm 10.14	67.17 \pm 1.49	79.45 \pm 0.77	51.77 \pm 13.22	59.70 \pm 1.15	66.45 \pm 0.54

TABLE IX: Comparison of gene deletion strategy prediction performance between two ablation variants—one using only metabolic inputs and the other using only gene inputs—across the three metabolic models under study. The best-performing results are highlighted in bold.

Metric	e_coli_core		iMM904		iML1515	
	Metabolite	Gene	Metabolite	Gene	Metabolite	Gene
Overall Accuracy (%)	56.05 \pm 0.57	62.14 \pm 0.45	64.86 \pm 0.58	72.97 \pm 0.46	54.05 \pm 0.57	61.16 \pm 0.44
Macro-Averaged Precision (%)	52.59 \pm 0.56	70.75 \pm 0.44	73.06 \pm 0.57	78.23 \pm 0.45	57.11 \pm 0.56	66.81 \pm 0.45
Macro-Averaged Recall (%)	51.76 \pm 0.57	41.38 \pm 0.48	65.64 \pm 0.56	69.49 \pm 0.44	54.82 \pm 0.57	61.40 \pm 0.45
Macro-Averaged F1 Score (%)	48.65 \pm 0.56	52.22 \pm 0.45	62.10 \pm 0.57	69.17 \pm 0.45	50.43 \pm 0.56	58.49 \pm 0.44
Macro-Averaged AUC (%)	51.64 \pm 0.84	61.51 \pm 0.81	62.47 \pm 0.83	71.88 \pm 0.74	53.28 \pm 0.71	60.85 \pm 0.59

F1 score, and AUC, DBgDel achieved the highest performance with 71.71%, 72.15%, 70.14%, and 71.88%, respectively. In comparison, the BPM and DNN baselines showed lower and less balanced results: BPM achieved 56.68%, 71.04%, 61.35%, and 56.74%, while DNN achieved 64.35%, 64.78%, 60.19%, and 62.04%, respectively.

Table IX item ‘e_coli_core’ summarizes the performance comparison between two ablation variants of DBgDel, i.e., with only input SMILES data of metabolites or AA sequence of genes, in the context of targeting GCP-possible metabolites of the *e_coli_core* metabolic model. When utilizing only SMILES data of metabolites as input, the overall accuracy achieved is 56.05%. In comparison, utilizing only AA sequence data of genes as input achieved a better overall accuracy of 62.14%. Regarding the macro-averaged precision, recall, F1 score, and AUC, the variant with only input of metabolite SMILES data achieved results of 52.59%, 51.76%, 48.65%, and 51.64% respectively. In comparison, the variant with only input of gene AA sequence data showed less balanced performance with 70.75%, 41.38%, 52.22%, and 61.51% respectively.

For iMM904: Table VIII item ‘iMM904’ summarizes the performance comparison among the proposed framework DBgDel and baseline methods in the context of targeting GCP-possible metabolites of *iMM904* metabolic model. Regarding overall accuracy, DBgDel achieved the highest score of 79.78% across all tested target metabolites. In comparison, the BPM and DNN baselines achieved 57.27% and 69.98%, respectively. Regarding the macro-averaged precision, recall, F1 score, and AUC, DBgDel achieved the highest performance with 78.29%, 77.08%, 77.25%, and 79.45%, respectively. In comparison, the BPM and DNN baselines showed lower and less balanced results: BPM achieved 54.38%, 73.29%, 60.00%, and 53.06%, while DNN achieved 72.48%, 67.84%, 64.20%, and 67.17%, respectively.

Table IX item ‘iMM904’ summarizes the performance comparison between two ablation variants of DBgDel, in the context of targeting GCP-possible metabolites of the *iMM904* metabolic model. When utilizing only SMILES data of metabolites as input, the overall accuracy achieved is 64.86%. In

comparison, utilizing only AA sequence data of genes as input achieved a better overall accuracy of 72.97%. Regarding the Macro-averaged precision, recall, F1 score, and AUC, the variant with only input of metabolite SMILES data achieved results of 73.06%, 65.64%, 62.10%, and 62.47% respectively. In comparison, the variant with only input of gene AA sequence data showed better performance with 78.23%, 69.49%, 69.17%, and 71.88% respectively.

For iML1515: Table VIII item ‘iML1515’ summarizes the performance comparison between the proposed framework DBgDel and the baseline method in the context of targeting GCP-possible metabolites of *iML1515* metabolic model. Regarding overall accuracy, DBgDel achieved the highest score of 67.24% across all tested target metabolites. In comparison, the BPM and DNN baselines achieved 54.21% and 60.44%, respectively. Regarding the macro-averaged precision, recall, F1 score, and AUC, DBgDel achieved the highest performance with 69.59%, 63.76%, 62.59%, and 66.45%, respectively. In comparison, the BPM and DNN baselines showed lower and less balanced results: BPM achieved 54.04%, 60.03%, 55.15%, and 51.77%, while DNN achieved 63.96%, 62.09%, 58.11%, and 59.70%, respectively.

Table IX item ‘iML1515’ summarizes the performance comparison between two ablation variants of DBgDel, in the context of targeting GCP-possible metabolites of the *iML1515* metabolic model. When utilizing only SMILES data of metabolites as input, the overall accuracy achieved is 54.05%. In comparison, utilizing only AA sequence data of genes as input achieved a better overall accuracy of 61.16%. Regarding the macro-averaged precision, recall, F1 score, and AUC, the variant with only input of metabolite SMILES data achieved results of 57.11%, 54.82%, 50.43%, and 53.28% respectively. In comparison, the variant with only input of gene AA sequence data showed better performance with 66.81%, 61.40%, 58.49%, and 60.85% respectively.

V. DISCUSSION AND CONCLUSION

In this study, we formulate the problem of gene deletion strategy prediction and propose a framework, DBgDel, to

solve it in genome-scale metabolic models. DBgDel leverages deep learning algorithms to learn from sequential gene and metabolite data, enabling the automatic prediction of gene deletion strategies for growth-coupled production.

In the computational experiments, we compared DBgDel with baseline methods on three constraint-based models of different scales. Experimental results demonstrate the feasibility of using DBgDel to predict gene deletion strategies across metabolic models of varying scales in an entirely data-driven manner, and DBgDel outperforms the baseline method across all five evaluation metrics. Specifically, the overall accuracy of DBgDel for *e_coli_core*, iMM904, and iML1515 were 71.90%, 79.78%, and 67.24%, respectively, representing substantial improvements of 14.69%, 22.52%, and 13.03% over the non-learning baseline method. At the same time, it achieves a higher AUC with balanced precision and recall in predicting gene statuses as deleted or non-deleted, while maintaining a low standard deviation—an outcome the baseline methods fail to achieve. The performance of DBgDel across the three metabolic models also demonstrates its applicability to metabolic models of varying scales and its robustness to limited training data. Notably, despite the *e_coli_core* model having only about 10% of the available deletion strategies data compared to the *iML1515* model, DBgDel remains effective. In addition to the detailed experiments on deep learning baselines (i.e., DNN), we also tested conventional machine learning methods such as Random Forest. However, its performance showed no consistent improvement over the BMP baseline in large-scale metabolic models. This further demonstrates the advantage of deep learning methods for this task.

We also experimented with two ablation variants of the proposed framework to analyze the impact of the two proposed input data types—metabolites and genes—on the performance of the gene deletion strategy prediction task. The experimental results demonstrate that both input types are essential for optimal performance. Using only a single data type results in consistent performance degradation across all metabolic models under study. Specifically, using only SMILES data for metabolites leads to an average overall accuracy drop of 18.86%, while using only AA sequence data for genes results in an 11.76% drop. This demonstrates that both proposed input types are essential for optimal gene deletion strategy prediction task performance.

We argue that the core strength of DBgDel lies in its modular design, which enables the parallel execution of metabolites and gene representation learning tasks (Meta-M and Gene-M), followed by feature integration for pairwise gene deletion status prediction (Pred-M). This design provides greater flexibility, allowing DBgDel to be extended to other deep learning models that can effectively perform the designed representation learning tasks.

While this work does not focus on selecting or refining specific deep learning models for learning from metabolites and gene sequence input data, we use a classical sequential data learning model, LSTM, as the default to demonstrate and benchmark the framework's feasibility. Although advanced deep learning models, such as recent large language models (LLMs) and other foundation models specialized for molecular or protein sequences [38], [39], often achieve superior performance in representation learning tasks, they come with a significantly larger number of parameters compared to classical sequential models [40], [41]. This results in higher training and inference costs, both in terms of time and memory demands.

Therefore, in practical applications, the choice of deep learning model within the proposed framework should consider both effectiveness and computational cost.

It is also worth noting that a genome-scale constraint-based model inherently possesses a complex network structure within both its metabolic network and GPR rule components, as defined in Section II-A. However, these graph-based relationships, such as the upstream-downstream connections among metabolites and the associations between genes and reactions, are not explicitly modeled in the proposed DBgDel framework. A reasonable assumption is that these intrinsic graph structures contain valuable information for solving the gene strategy prediction task formulated in this study while still adhering to the problem setting given in Section II-C. The lack of such graphical information may hinder the neural network's ability to capture the relationships between metabolites, thereby preventing the proposed framework from achieving optimal performance. While incorporating this information would require more complex deep learning models with larger parameter counts and advanced implementation techniques, graph-based modeling of relationships between metabolic model elements holds promise for future advances in data-driven strain design.

In future work, we will benchmark the performance of various deep learning models for metabolite and gene representation learning within the proposed framework across metabolic models from a wider range of species. Additionally, we will explore incorporating extended metabolic model information, such as metabolic network structure or reaction bounds, to enhance the performance of the gene deletion strategy prediction task.

VI. ACKNOWLEDGMENTS

This work was supported in part by JSPS, KAKENHI under Grant 23K20386, and JST SPRING, Grant Number JP-MJSP2110.

REFERENCES

- [1] Otero-Muras, I. & Carbonell, P. Automated engineering of synthetic metabolic pathways for efficient biomanufacturing. *Metabolic Engineering* **63**, 61–80 (2021).
- [2] García-Jiménez, B., Torres-Bacete, J. & Nogales, J. Metabolic modelling approaches for describing and engineering microbial communities. *Computational and Structural Biotechnology Journal* **19**, 226–246 (2021).
- [3] Foster, C. J., Wang, L., Dinh, H. V., Suthers, P. F. & Maranas, C. D. Building kinetic models for metabolic engineering. *Current Opinion in Biotechnology* **67**, 35–41 (2021).
- [4] Toya, Y. & Shimizu, H. Flux analysis and metabolomics for systematic metabolic engineering of microorganisms. *Biotechnology advances* **31**, 818–826 (2013).
- [5] Pharkya, P. & Maranas, C. D. An optimization framework for identifying reaction activation/inhibition or elimination candidates for overproduction in microbial systems. *Metabolic engineering* **8**, 1–13 (2006).
- [6] Vieira, V., Maia, P., Rocha, M. & Rocha, I. Comparison of pathway analysis and constraint-based methods for cell factory design. *BMC bioinformatics* **20**, 1–15 (2019).
- [7] Ranganathan, S., Suthers, P. F. & Maranas, C. D. Optforce: an optimization procedure for identifying all genetic manipulations leading to targeted overproductions. *PLoS computational biology* **6**, e1000744 (2010).
- [8] Rockwell, G., Guido, N. J. & Church, G. M. Redirector: designing cell factories by reconstructing the metabolic objective. *PLoS computational biology* **9**, e1002882 (2013).
- [9] Yang, L., Cluett, W. R. & Mahadevan, R. Emilio: a fast algorithm for genome-scale strain design. *Metabolic engineering* **13**, 272–281 (2011).

[10] Egen, D. & Lun, D. S. Truncated branch and bound achieves efficient constraint-based genetic design. *Bioinformatics* **28**, 1619–1623 (2012).

[11] Lewis, N. E. *et al.* Omic data from evolved *e. coli* are consistent with computed optimal growth from genome-scale models. *Molecular systems biology* **6**, 390 (2010).

[12] Gu, D., Zhang, C., Zhou, S., Wei, L. & Hua, Q. Idealknock: a framework for efficiently identifying knockout strategies leading to targeted overproduction. *Computational biology and chemistry* **61**, 229–237 (2016).

[13] Ohno, S., Shimizu, H. & Furusawa, C. Fastpros: screening of reaction knockout strategies for metabolic engineering. *Bioinformatics* **30**, 981–987 (2014).

[14] Tamura, T. Grid-based computational methods for the design of constraint-based parsimonious chemical reaction networks to simulate metabolite production: Gridprod. *BMC bioinformatics* **19**, 1–9 (2018).

[15] Tamura, T., Muto-Fujita, A., Tohsato, Y. & Kosaka, T. Gene deletion algorithms for minimum reaction network design by mixed-integer linear programming for metabolite production in constraint-based models: gdel_minrn. *Journal of Computational Biology* **30**, 553–568 (2023).

[16] Trinh, C. T., Unrean, P. & Srienc, F. Minimal *escherichia coli* cell for the most efficient production of ethanol from hexoses and pentoses. *Applied and environmental microbiology* **74**, 3634–3643 (2008).

[17] Schneider, P., von Kamp, A. & Klamt, S. An extended and generalized framework for the calculation of metabolic intervention strategies based on minimal cut sets. *PLoS computational biology* **16**, e1008110 (2020).

[18] Banerjee, D. *et al.* Genome-scale metabolic rewiring improves titers rates and yields of the non-native product indigoidine at scale. *Nature communications* **11**, 5385 (2020).

[19] Tamura, T. Metnetcomp: Database for minimal and maximal gene-deletion strategies for growth-coupled production of genome-scale metabolic networks. *IEEE/ACM Transactions on Computational Biology and Bioinformatics* (2023).

[20] Yang, Z. & Tamura, T. Dbgdel: Database-enhanced gene deletion framework for growth-coupled production in genome-scale metabolic models. *IEEE Transactions on Computational Biology and Bioinformatics* (2025).

[21] LeCun, Y., Bengio, Y. & Hinton, G. Deep learning. *nature* **521**, 436–444 (2015).

[22] Costello, Z. & Martin, H. G. A machine learning approach to predict metabolic pathway dynamics from time-series multiomics data. *NPJ systems biology and applications* **4**, 1–14 (2018).

[23] Li, F. *et al.* Deep learning-based k cat prediction enables improved enzyme-constrained model reconstruction. *Nature Catalysis* **5**, 662–672 (2022).

[24] Yan, J. *et al.* Multi-modal imitation learning for arc detection in complex railway environments. *IEEE Transactions on Instrumentation and Measurement* (2025).

[25] Cheng, Y. *et al.* Surrogate modeling of pantograph-catenary system interactions. *Mechanical Systems and Signal Processing* **224**, 112134 (2025).

[26] Orth, J. D., Thiele, I. & Palsson, B. Ø. What is flux balance analysis? *Nature biotechnology* **28**, 245–248 (2010).

[27] Schneider, P., Mahadevan, R. & Klamt, S. Systematizing the different notions of growth-coupled product synthesis and a single framework for computing corresponding strain designs. *Biotechnology Journal* **16**, 2100236 (2021).

[28] Alter, T. B. & Ebert, B. E. Determination of growth-coupling strategies and their underlying principles. *BMC bioinformatics* **20**, 1–17 (2019).

[29] Sattarov, B. *et al.* De novo molecular design by combining deep autoencoder recurrent neural networks with generative topographic mapping. *Journal of chemical information and modeling* **59**, 1182–1196 (2019).

[30] Abbasi, K. *et al.* Deepcda: deep cross-domain compound–protein affinity prediction through lstm and convolutional neural networks. *Bioinformatics* **36**, 4633–4642 (2020).

[31] Sønderby, S. K., Sønderby, C. K., Nielsen, H. & Winther, O. Convolutional lstm networks for subcellular localization of proteins. In *Algorithms for Computational Biology: Second International Conference, AlCoB 2015, Mexico City, Mexico, August 4–5, 2015, Proceedings* **2**, 68–80 (Springer, 2015).

[32] Vaswani, A. *et al.* Attention is all you need. *Advances in neural information processing systems* **30** (2017).

[33] Shi, X. *et al.* Convolutional lstm network: A machine learning approach for precipitation nowcasting. *Advances in neural information processing systems* **28** (2015).

[34] Orth, J. D., Fleming, R. M. & Palsson, B. Ø. Reconstruction and use of microbial metabolic networks: the core *escherichia coli* metabolic model as an educational guide. *EcoSal plus* **4**, 10–1128 (2010).

[35] Mo, M. L., Palsson, B. Ø. & Herrgård, M. J. Connecting extracellular metabolomic measurements to intracellular flux states in yeast. *BMC systems biology* **3**, 1–17 (2009).

[36] Monk, J. M. *et al.* iml1515, a knowledgebase that computes *escherichia coli* traits. *Nature biotechnology* **35**, 904–908 (2017).

[37] Paszke, A. Pytorch: An imperative style, high-performance deep learning library. *arXiv preprint arXiv:1912.01703* (2019).

[38] Ahmad, W., Simon, E., Chithrananda, S., Grand, G. & Ramsundar, B. Chemberta-2: Towards chemical foundation models. *arXiv preprint arXiv:2209.01712* (2022).

[39] Madani, A. *et al.* Large language models generate functional protein sequences across diverse families. *Nature biotechnology* **41**, 1099–1106 (2023).

[40] Thirunavukarasu, A. J. *et al.* Large language models in medicine. *Nature medicine* **29**, 1930–1940 (2023).

[41] Zhang, Q. *et al.* Scientific large language models: A survey on biological & chemical domains. *ACM Comput. Surv.* **57** (2025). URL <https://doi.org/10.1145/3715318>.